A&A 553, A72 (2013)
DOI: 10.1051/0004-6361/201220453

Astronomy & Astrophysics

The NGC 1614 interacting galaxy

Molecular gas feeding a "ring of fire"

S. König[1,2], S. Aalto[3], S. Muller[3], R. J. Beswick[4], and J. S. Gallagher III[5]

[1] Institut de Radioastronomie Millimétrique, 300 rue de la Piscine, Domaine Universitaire, 38406 Saint-Martin d'Hères, France
e-mail: koenig@iram.fr
[2] Dark Cosmology Centre, Niels Bohr Institute, University of Copenhagen, Juliane Maries Vej 30, 2100 Copenhagen, Denmark
[3] Chalmers University of Technology, Department of Radio and Space Science, Onsala Space Observatory, 43992 Onsala, Sweden
[4] University of Manchester, Jodrell Bank Centre for Astrophysics, Oxford Road, Manchester, M13 9PL, UK
[5] Department of Astronomy, University of Wisconsin, 475 N Charter Street, Madison, WI, 53706, USA

Received 27 September 2012 / Accepted 1 March 2013

ABSTRACT

Minor mergers frequently occur between giant and gas-rich low-mass galaxies and can provide significant amounts of interstellar matter to refuel star formation and power active galactic nuclei (AGN) in the giant systems. Major starbursts and/or AGN result when fresh gas is transported and compressed in the central regions of the giant galaxy. This is the situation in the starburst minor merger NGC 1614, whose molecular medium we explore at half-arcsecond angular resolution through our observations of ^{12}CO (2−1) emission using the Submillimeter Array (SMA). We compare our ^{12}CO (2−1) maps with optical and Paα, *Hubble* Space Telescope and high angular resolution radio continuum images to study the relationships between dense molecular gas and the NGC 1614 starburst region. The most intense ^{12}CO emission occurs in a partial ring with ∼230 pc radius around the center of NGC 1614, with an extension to the northwest into the dust lane that contains diffuse molecular gas. We resolve ten giant molecular associations (GMAs) in the ring, which has an integrated molecular mass of $\sim 8 \times 10^8$ $M_\odot$. Our interferometric observations filter out a large part of the ^{12}CO (1−0) emission mapped at shorter spacings, indicating that most of the molecular gas is diffuse and that GMAs only exist near and within the circumnuclear ring. The molecular ring is uneven with most of the mass on the western side, which also contains GMAs extending into a pronounced tidal dust lane. The spatial and kinematic patterns in our data suggest that the northwest extension of the ring is a cosmic umbilical cord that is feeding molecular gas associated with the dust lane and tidal debris into the nuclear ring, which contains the bulk of the starburst activity. The astrophysical process for producing a ring structure for the final resting place of accreted gas in NGC 1614 is not fully understood, but the presence of numerous GMAs suggests an orbit-crowding or resonance phenomenon. There is some evidence that star formation is progressing radially outward within the ring, indicating that a self-triggering mechanism may also affect star formation processes. The net result of this merger therefore very likely increases the central concentration of stellar mass in the NGC 1614 remnant giant system.

Key words. galaxies: active – galaxies: evolution – galaxies: individual: NGC 1614 – galaxies: starburst – ISM: molecules

1. Introduction

Merger events, i.e., close interactions of galaxy pairs, have a deep impact on the evolution of galaxies through the triggering of active galactic nuclei (AGN) and starburst activity. Studies of interacting galaxies often focus on major mergers (nearly equal mass spirals) (e.g. Toomre & Toomre 1972; Tacconi et al. 2002; Dasyra et al. 2006; Jesseit et al. 2007; Somerville et al. 2008; Kormendy et al. 2009) and their evolution, although minor mergers most likely constitute the bulk of all galaxy interactions (e.g. Toth & Ostriker 1992; Zaritsky 1995; Hunsberger et al. 1996). Investigating how the gas is feeding starburst and AGN activities in these objects is therefore paramount for understanding the overall evolution of the Universe. Although there is still no consensus about what powers the emission in low ionization nuclear emission line regions (LINERs), nuclear starburst, AGN activity, and shocks are three major candidates (e.g. Veilleux et al. 1999; Ho 1999; Terashima et al. 2000; Alonso-Herrero et al. 2000; Monreal-Ibero et al. 2006). Bar-driven inflow of gas in galaxies has been suggested to trigger nuclear starbursts, and the feeding of AGNs (e.g. Simkin et al. 1980; Scoville et al. 1985). However, the radial inflow of gas along the bar may be slowed down at certain radii, which are often associated with inner Lindblad resonances (ILR, Combes 1988b; Shlosman et al. 1989).

NGC 1614 is an excellent example of a minor merger with a spectacular morphology and intense nuclear activity. The nucleus of this galaxy displays characteristics of containing an intense nuclear starburst region and may also contain some level of AGN activity. NGC 1614 (SB(s)c pec, de Vaucouleurs et al. 1991) is a luminous infrared galaxy (LIRG, Sanders et al. 2003) at a distance of 64 Mpc (de Vaucouleurs et al. 1991, for $H_0 = 75$ km s^{-1} Mpc^{-1}; $1'' = 310$ pc). Most of the starburst activity can be attributed to the interaction with a companion galaxy located in the tidal tail to the southwest of the nucleus of NGC 1614 (Neff et al. 1990; Olsson et al. 2010; Väisänen et al. 2012). A mass ratio of ∼5:1−3:1 has been found for this minor merger system (Väisänen et al. 2012). Its nuclear optical spectrum shows both starburst and LINER activity. A circumnuclear ring (r = 300 pc, see e.g. Fig. 1) in NGC 1614, seen in tracers such as Paα (Alonso-Herrero et al. 2001, along with an

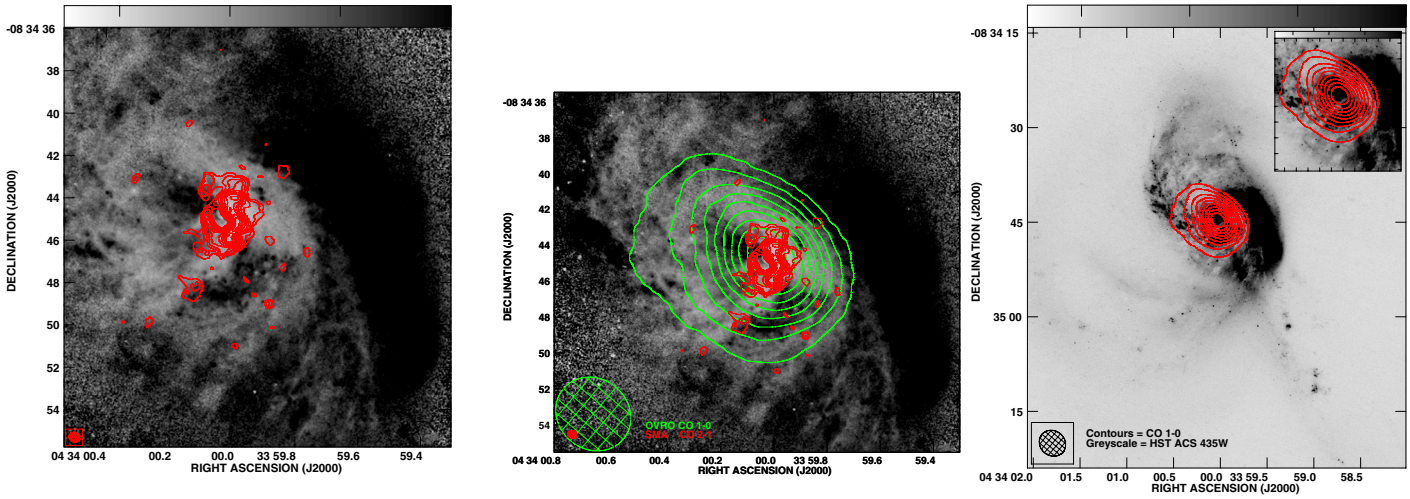

Fig. 1. Overlay of the CO (2−1) integrated intensity emission (*left*, Olsson et al. 2010) and of the CO (2−1) and low-resolution CO (1−0) (*middle*, Olsson et al. 2010) integrated intensity emission on the HST *F435W*/*F814W* filter color-map image, and overlay of the CO (1−0) emission (*right*) on an HST *F435W* filter image on the scale of the whole merger system. Note how well the CO (2−1) emission distribution correlates with the dust lanes (light gray colors on the *left-hand side and the middle in this figure*) and that the position of the emission peak of the CO (1−0) distribution coincides with the main part of the dust emission in this region. The CO beam sizes (CO (2−1): 0.50″ × 0.44″, CO (1−0): 4.44″ × 4.10″) are shown in the lower left corners.

identification in $H - K$ imaging), radio continuum (Olsson et al. 2010) and polycyclic aromatic hydrocarbons (PAHs; Väisänen et al. 2012), hosts a very young starburst (5−10 Myr, top-heavy initial mass function, Puxley & Brand 1999) while an older (>10 Myr) starburst resides in the nucleus – possibly encircling an AGN. Alonso-Herrero et al. (2001) claimed that the ring is the cause of "wildfire" starburst activity propagating from the nucleus in an outward direction through cloud-cloud collisions and winds, while Olsson et al. (2010) instead suggest that the ring is the result of a resonance, possibly linked to a stellar bar.

Though NGC 1614 has intense nuclear activity, its spiral arms are devoid of molecular gas, which raises the question how the gas reached the nucleus. Numerical simulation studies of minor- or intermediate mergers show that gas brought in by the disturbing companion galaxy is generally found at large radii in the merger remnant (Bournaud et al. 2005). Gas returns to the system from tidal tails and often forms rings – polar, inclined or equatorial – that will appear as dust lanes when seen edge-on.

One dominant feature of the optical morphology of NGC 1614 is the prominent dust lane that crosses the galaxy just north of the central activity. A considerable fraction of the CO (1−0) emission resides in this dust lane and is not directly involved in the nuclear activity. The OVRO CO (1−0) observations (2.5″ resolution) presented by Olsson et al. (2010) were unable to spatially resolve the molecular structure of the inner region.

Furthermore, a spatial correlation between CO emission and 1.4 GHz radio continuum is commonly observed in galaxies. This is not the case for NGC 1614, however. There is probably no star formation associated with the dust lane – possibly because gas is being funneled along it, with the resulting shear, which prevents efficient star formation. A similar CO-dust lane correlation has been found for another minor merger, the Medusa merger, for which the gas in the dust lane is suggested to be diffuse because of the gas-funneling (Aalto & Hüttemeister 2000).

Here we present a study of the ^{12}CO emission toward the center of NGC 1614. In Sect. 2 we describe the observations and data reduction, and in Sect. 3 we present the results.

2. Observations

NGC 1614 was observed with the Submillimeter Array (SMA) in the ^{12}CO (2−1) and ^{13}CO (2−1) transitions. We obtained one full track (10 h), between 22 LST and 08 LST, in the SMA's most extended configuration, the Vext array configuration, with a resolution of 0.5″on 26 July 2010, which provided baselines between 68 m up to ∼509 m. Our map is therefore sensitive to structures smaller than 2.4″. Using the 230 GHz band receiver in conjunction with the DR 128 correlator (DR = default resolution) mode with a bandwidth of 4 GHz provided channel widths of 0.8125 MHz, resulting in a velocity coverage of 5305.7 km s^{-1} with a channel separation of 1.1 km s^{-1}. For data analysis a final channel width of 21 km s^{-1} was used. The 4 GHz band was centered at a rest frequency of 226.931 GHz (corresponding to a central velocity of $v_{\rm opt,hel}$ = 4778 km s^{-1}) for the upper side band (USB). The system noise temperature $T_{\rm sys}$ ranged between 80 and 170 K. During the observations several sources were used as calibrators: 3C 454.3 as the band pass calibrator, the nearby source 0423-013 for the phase calibration of NGC 1614, and Neptune and Callisto as flux calibrators.

We reduced and analyzed the data using the MIR IDL and GILDAS[1] Mapping data reduction software packages. For the CO (2−1) line the synthesized beam resulting from natural weighting is 0.50″ × 0.44″ with a position angle of 54°. For the 1 mm continuum observations the smoothed synthesized beam from natural weighting is 0.96″ × 0.96″.

To provide high resolution images of the optical structure of NGC 1614, we obtained pipeline-reduced *Hubble* Space Telescope images taken with the Advanced Camera for Surveys in the *F435W* and *F814W* filters (see Fig. 1). These data were obtained as part of program G0-10592 (A. Evans, P. I.) and have an angular resolution of 0.05 arcsec pixel^{-1} corresponding to a linear scale of ∼15 pc pixel^{-1}.

[1] http://www.iram.fr/IRAMFR/GILDAS

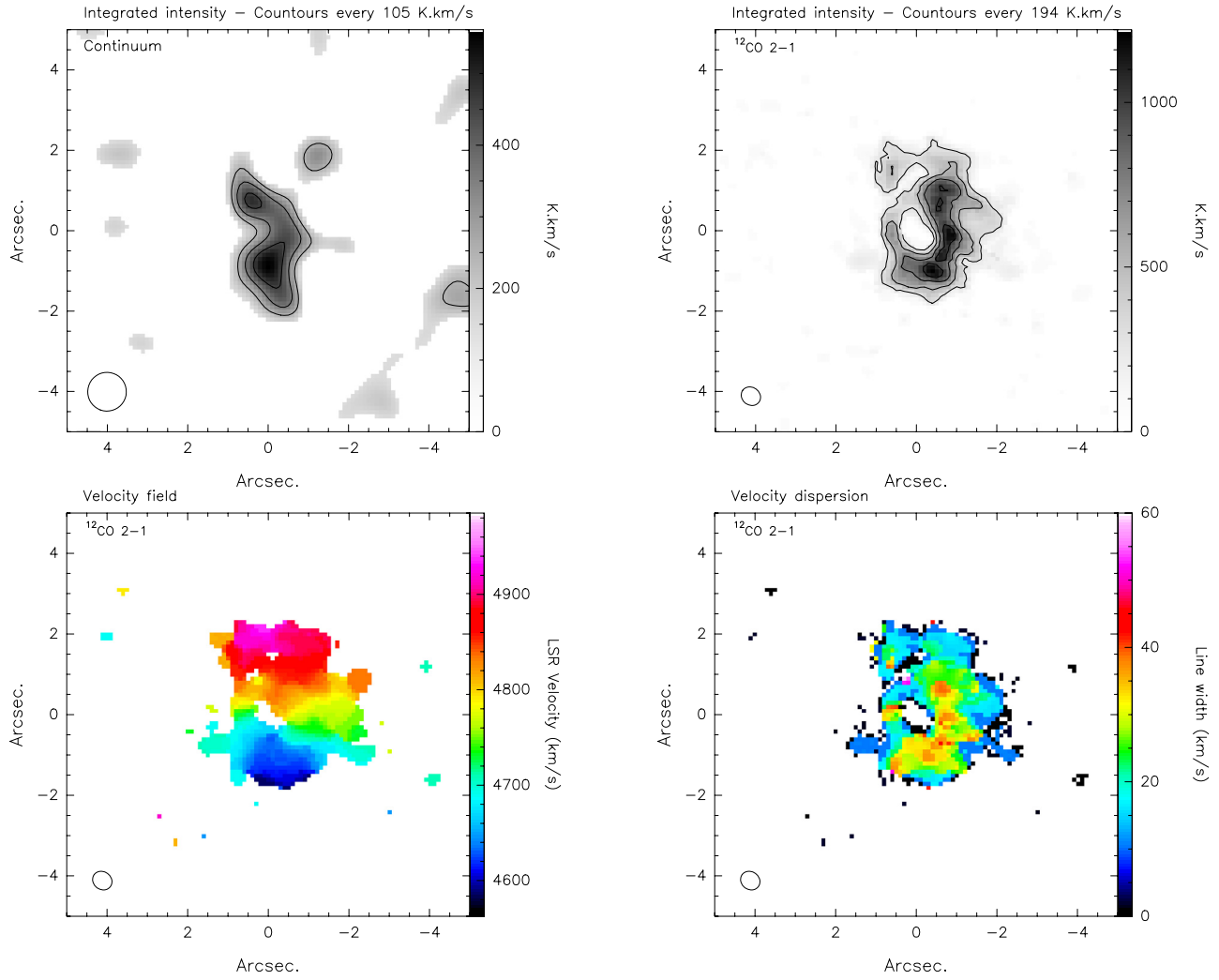

Fig. 2. Smoothed naturally weighted SMA 1.3 mm continuum (*upper left*) in NGC 1614. The noise level is 0.71 mJy/beam. Contours start at 1.5σ in steps of 1.1σ. Integrated intensity map (*upper right*), velocity field (*bottom left*), and velocity dispersion (*bottom right*) of the CO (2–1) emission in NGC 1614. The noise level is 6.16 mJy/beam. Contours for the integrated intensity map start at 4σ in steps of 4σ, contours for the velocity field and velocity dispersion start at 5σ. The velocity range plotted in the velocity field is between ~4520 km s^{-1} and ~4985 km s^{-1}. The beam sizes are indicated in the lower left corner of each plot and are listed in Sect. 2.

3. Results

3.1. 1.3 mm continuum

The 1.3 mm continuum map (Fig. 2, upper left panel) shows centrally peaked emission with a flux density of $\sim 19 \pm 6$ mJy, which agrees well with the values for the 1.3 mm continuum obtained by Wilson et al. (2008), who observed a total of 21 ± 3 mJy was observed. Our 1.3 mm continuum map appears to be comprised of two components and has a box-like shape that is consistent with the structure Wilson et al. (2008) observed in their 1.3 mm continuum map.

3.2. ^{12}CO and ^{13}CO (2–1)

3.2.1. CO (2–1) integrated intensity

The upper right panel of Fig. 2 shows the ^{12}CO (2–1) integrated intensity map derived from our data. The ^{13}CO (2–1) line was not detected at 3σ a level of 17.26 Jy km s^{-1} in these SMA observations, which agrees with values from Wilson et al. (2008), although they detected the line. The higher spatial resolution of our Vext data might lead to a non-detection of lower density ^{13}CO (2–1) gas that Wilson et al. (2008) were able to find with their lower resolution data. The ^{12}CO emission appears as a ring-like structure without emission at its center, with a gas component, that might connect to the dust lane (hereafter *umbilical cords*), to the northwest and an extension of lower surface brightness gas to the north (see Fig. 3). Both within and slightly beyond this ring structure hot spots of ^{12}CO are clearly identifiable. These are discussed in Sect. 3.4.

The highest flux density is 203 Jy km s^{-1} (Table 1). A comparison to previous observations of Wilson et al. (2008) shows us that we recovered only about ~30% of the total flux density. We find a clear asymmetry in the east-west gas distribution of the ring-like structure, or possibly tightly wound spiral arms. The eastern side has much less gas than the western part. The intensity ratio is I(west)/I(east) ~ 2.7.

Using a CO-to-H_2 conversion factor of $X_{CO} = 3 \times 10^{20}$ cm^{-2} (K km s^{-1})$^{-1}$ (Narayanan et al. 2011) results in a molecular mass of 2.1×10^9 $M_\odot$ for the whole system. If we consider the *umbilical cords* (Fig. 3) as a separate mass entity, the ring itself has a gas mass of 8.3×10^8 $M_\odot$ (Table 1).

Table 1. Properties of the observed emission in NGC 1614.

	Integrated flux		Mass[a]		
	^{12}CO (2−1)	^{13}CO (2−1)	M (^{12}CO 2−1)	M (^{13}CO 2−1)	M (1.3 mm continuum)
	[Jy km s^{-1}]	[Jy km s^{-1}]	[$M_\odot$]	[$M_\odot$]	[$M_\odot$]
Whole system	203.3 ± 9.8	<7.7	2.12×10^9	$<2.74\times10^5$	1.03×10^9
Ring	65.4 ± 6.9	<1.0	8.29×10^8	$<3.25\times10^4$	3.94×10^8
Dust lane connection	25.8 ± 5.3	<1.0	2.54×10^8	$<5.40\times10^4$	2.33×10^7
Northern extension	22.7 ± 6.2	<3.0	3.32×10^8	$<1.39\times10^5$	1.25×10^8

Notes. [(a)] We adopted a conversion factor of 3×10^{20} cm^{-2} (K km s^{-1})$^{-1}$.

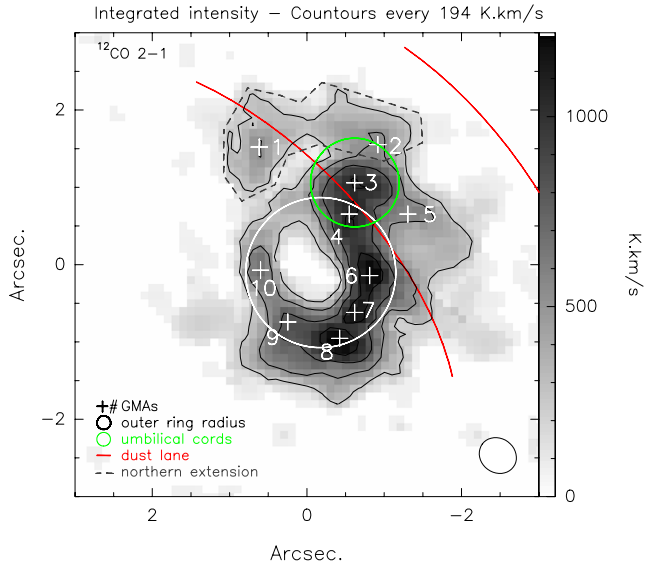

Fig. 3. Description of important geometrical structures in the integrated intensity map of the CO (2−1) emission in NGC 1614. The extent and position of the starburst ring, the *northern extension*, the umbilical cords (connection to the dust lane) to the north and west of the ring that contain GMAs 2, 3, 4, and 5 and the GMAs are indicated. To clearly distinguish between the GMAs and their positions, their respective numbers are indicated as well.

3.2.2. Missing flux and the structure of the CO emission

In our CO (2−1) integrated intensity map we recover only 30% of the CO (2−1) flux density of the low-resolution SMA observations of Wilson et al. (2008), thus we most likely only see the most compact structures. A comparison of their lower resolution CO (2−1) map and the structures of the high- and low-resolution CO (1−0) observed by Olsson et al. (2010) shows remarkable similarities in the morphology. Hence we suggest that the bulk of the missing flux is located in the northern crossing dust lane (see also Fig. 1) – but also in structures that trace the beginning of the southern arm and emission to the east of the ring.

3.2.3. CO (2−1) velocity field, velocity dispersion, and position–velocity diagrams

The velocity field, with velocities ranging from ~4520.42 km s^{-1} to 4985.31 km s^{-1}, is shown in Fig. 2 (bottom left panel). It shows a behavior typical for solid-body rotation, for which the probable connection to the dust lane follows the behavior of the gas in the ring.

The velocity dispersion distribution of NGC 1614 shows several peaks (Fig. 2, bottom right panel). At these peaks the velocity dispersions rise to 43−51 km s^{-1} compared to the underlying material, which only shows dispersion values between ~15 and ~33 km s^{-1}. The velocity dispersion might be biased by missing extended structures in our map. This probably does not affect the dispersion of the ring itself because it is compact.

In Fig. 4 the position velocity diagrams along the major (north to south) and minor (east to west) axes are shown. They were obtained by averaging over a 1″-wide slit positioned along the major and minor axes centered on the center of the ring. The pattern for solid-body rotation seen in the velocity field is also reflected in the major axis position velocity diagram. In the minor axis position velocity diagram we clearly see a difference between the eastern and the western part of the ring, with the majority of the gas residing in the western part of the ring.

Table 2. Properties of the molecular ring in NGC 1614.

Property	
Ring center coordinates	RA: 04:34:00.036, Dec: −08:34:45.08
Molecular mass $M_{\rm mol}$	8.29×10^8 $M_\odot$
Dynamical mass $M_{\rm dyn}$	1.85×10^9 $M_\odot$
West-east intensity ratio	2.7
Radius	0.75″ (~231 pc)
GMAs on the ring	6
GMAs off the ring	4

3.2.4. ^{12}CO/^{13}CO (2−1) ratio

To estimate the ^{12}CO/^{13}CO (2−1) ratio we used the integrated intensity maps of ^{12}CO (2−1) and ^{13}CO (2−1) integrated over the same velocity range and determined the average flux densities (flux density for ^{13}CO from the 3σ rms noise value) within the same polygon for both transitions. The resulting lower limit for the flux density ratio is ^{12}CO / ^{13}CO (2−1) > 15. An investigation of the spectra of Wilson et al. (2008) showed that the ^{12}CO/^{13}CO (2−1) line ratio for the peak (central) flux density is ~22, while the ratio for the integrated flux density (in the whole map) is ~38. One can see from their data that the ^{13}CO (2−1) flux density hardly rises going from peak flux densities to integrated intensities, while the ^{12}CO (2−1) flux densities increase by more than a factor of 2. From this it seems that the ^{12}CO/^{13}CO (2−1) ratio is increasing with radius in NGC 1614, a notion that should be confirmed at higher sensitivity and resolution; this would be reminiscent of the situation in the Medusa minor merger (NGC 4194, Aalto et al. 2010) and the molecular ring in NGC 6946 (Meier & Turner 2004). This is discussed again briefly in Sect. 4.1.2.

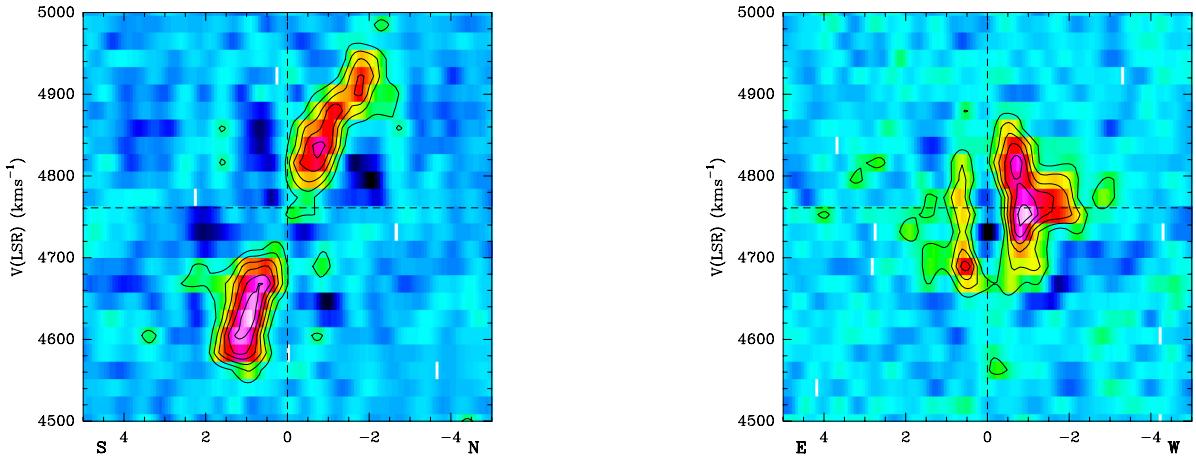

Fig. 4. ^{12}CO (2−1) position–velocity diagrams along the major (north-south, *left*) and the minor (east-west, *right*) axes of NGC 1614. The contour levels start at 3σ in steps of 3σ. The colors range from 0.1 to 0.28 mJy/beam for the major axis pv diagram and from 0.08 to 0.24 mJy/beam if the minor axis pv diagram.

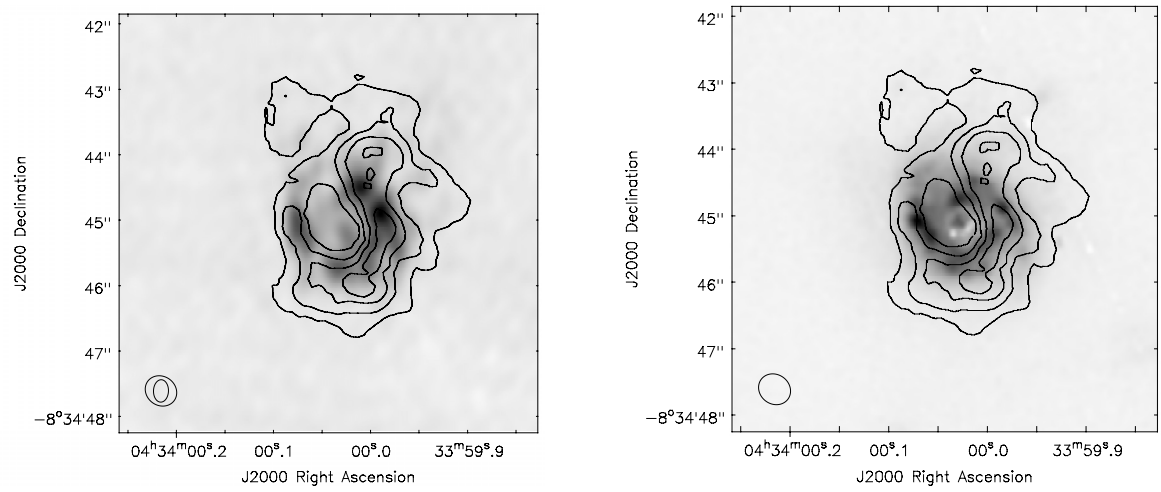

Fig. 5. Overlay of the CO (2−1) integrated intensity contours on the VLA 8 GHz emission (grayscale, *left*, Olsson et al. 2010) and overlay of the CO (2−1) integrated intensity emission (contours) on the Paα emission (grayscale, *right*, Olsson et al. 2010). The contour levels for the CO (2−1) emission are at 18.5, 41, 60.5, and 81% of the emission peak (same levels as in Fig. 2).

3.3. Properties of the molecular ring

Figures 2, 3, 5, and 6 show that we observe a ring-like structure in NGC 1614 with additional molecular gas emission to the north, the northeast, and the west. From the inside out, the structure evolves via *umbilical cords*, a gas component that possibly connects the ring to the dust lane located to the northeast, and then into a *northern extension* of lower surface density material (see Fig. 3). In contrast to the observations from Wilson et al. (2008) and Olsson et al. (2010), we clearly filtered out the more extended gas in this region. The angular resolution of our observations allowed us to resolve the width of the ring. In contrast to studies of NGC 1614 at other wavelengths, such as radio continuum and Paα, these ^{12}CO (2−1) observations detected no emission at the center of the ring (Fig. 5).

To obtain a better overview of the properties of the different components in this object, we also determined the masses for components outside the ring. We assumed a radius of the ring of 0.75″ (~231 pc) and a width of 0.5″. On this basis the mass for the ring is $M(\mathrm{H_2}) = 8.3 \times 10^8\ M_\odot$ (Table 2). The *umbilical cords* to the northeast have a mass of $M(\mathrm{H_2}) = 2.5 \times 10^8\ M_\odot$ and the mass of the *northern extension* is $M(\mathrm{H_2}) = 3.3 \times 10^8\ M_\odot$. We can now also calculate the dynamical mass for the ring by considering the radius and the width of the ring, as well as a rotational velocity of 187 km s^{-1}, estimated from the position velocity diagram. Because the angle of the ring to the plane of the sky is unknown, an uncertainty factor of cos(θ) has to be considered. Taking this into account, we determined the dynamical mass of the ring to be $M_{\mathrm{dyn}} = 1.85 \times 10^9 \cos(\theta)\ M_\odot$, which is a factor of ~2 higher than the molecular mass of the ring. The viewing angle to the molecular ring seems to be face-on, which justifies a cos(θ) of 1. A low inclination would not change the result drastically.

3.4. Giant molecular associations (GMAs) in NGC 1614

We found ten clumps in (GMA 4, GMA 6, GMA 7, GMA 8, GMA 9, GMA 10) and outside (GMA 1, GMA 2, GMA 3, GMA 5) the structure of the molecular ring (Fig. 3). They have masses between $M(\mathrm{H_2}) = 1.6 \times 10^7\ M_\odot$ and $M(\mathrm{H_2}) = 9.4 \times 10^7\ M_\odot$ (Table 3), which places these objects in the mass range for GMAs, so-called giant molecular associations (Vogel et al. 1988).

The velocity dispersion map (Fig. 2, bottom right panel) shows a rise in line widths at the positions of all GMAs in the ring (GMA 4, GMA 6, GMA 7, GMA 8, GMA 9). The dispersion values range between 31.1 km s^{-1} for GMA 2 and 72.9 km s^{-1}

Table 3. Properties of the identified GMAs.

GMA	RA(2000)	Dec(2000)	Size (diam.)[a]		v_0	Dispersion	Mass
	[h] [m] [s]	[°] [′] [″]	[″]	[pc]	[km s^{-1}]	[km s^{-1}]	[$M_\odot$]
GMAs in the ring:							
GMA 4	04:34:00.004	–08:34:44.37	0.6×1.0	250×336	4813 ± 7	61 ± 6	5.70×10^7
GMA 6	04:33:59.985	–08:34:45.08	0.6×0.9	195×268	4737 ± 5	64 ± 4	9.74×10^7
GMA 7	04:33:59.998	–08:34:45.57	0.8×1.1	261×341	4670 ± 7	38 ± 4	5.97×10^7
GMA 8	04:34:00.012	–08:34:45.97	1.3×0.8	390×260	4609 ± 6	73 ± 5	9.36×10^7
GMA 9	04:34:00.067	–08:34:45.56	0.6×1.2	192×368	4671 ± 6	54 ± 5	5.98×10^7
GMA 10	04:34:00.082	–08:34:45.01	0.5×0.7	168×204	4756 ± 7	40 ± 5	4.96×10^7
GMAs outside the ring:							
GMA 1	04:34:00.087	–08:34:43.45	0.6×1.1	197×326	4919 ± 7	57 ± 7	8.29×10^7
GMA 2	04:33:59.989	–08:34:43.38	1.1×0.5	336×157	4901 ± 7	31 ± 4	1.64×10^7
GMA 3	04:33:59.998	–08:34:43.97	0.8×1.1	250×336	4875 ± 5	53 ± 3	6.23×10^7
GMA 5	04:33:59.946	–08:34:44.37	1.8×0.6	566×180	4814 ± 7	48 ± 5	3.70×10^7

Notes. [(a)] The source size was determined by fitting an elliptical Gaussian to the position of the respective GMA in the uv table. The values given here represent the major and minor axis values resulting from the fitting procedure. The typical (average) error for the fit to the GMA sizes is about 20%.

for GMA 8. The GMAs outside the ring have an average dispersion of 47.0 km s^{-1}. The average dispersion for the GMAs in the ring is 55.0 km s^{-1}.

We ran a decomposition of the CO data cube into individual structures, using the task Gaussclumps (developed initially by Stutzki & Guesten 1990) in GILDAS/Mapping. The algorithm searches iteratively for 3D Gaussians in the data cube until it reaches a specified threshold value. To derive reliable results, we set this threshold to a value of 6σ. Under these conditions, the data cube can be decomposed into ten different Gaussian clumps, whose properties are listed in Table 3 while the positions are indicated in Fig. 3. Four of the five brightest clumps (GMA 4, GMA 6, GMA 8, and GMA 9), which we call GMAs, are clearly associated with the ring, where the CO emission is the brightest. The one GMA that is very bright (GMA 3) but does not lie in the ring is situated at the point where the molecular gas in the ring is connected to the dust lanes via the feeding lines (*umbilical cords*, see Sects. 4.1.1 and 4.1.2). The residual map is dominated by fainter emission located to the north of the ring. The resulting source sizes (Table 3) range between 168 pc × 204 pc and 390 pc × 260 pc for GMAs outside the molecular ring and 336 pc × 157 pc up to 566 pc × 180 pc for GMAs in the ring. Moreover, the GMAs outside the ring are more elliptical in shape, i.e., the major-to-minor axis ratio is much higher than for the GMAs in the ring, especially for the GMAs outside the ring that are situated in the dust lanes. Assuming spherical morphologies (for comparison purposes only), the average diameter of a GMA outside the ring is 273 ± 20 pc, whereas the GMAs in the ring show an average diameter of 259 ± 24 pc.

4. Discussion

4.1. Origin of the ring

4.1.1. "Feeding" of the ring: the connection to the dust lanes

Bournaud et al. (2005) found that in minor mergers gas brought in by a disturbing galaxy companion is generally found at large radii in the merger remnant. The gas returns to the system via tidal tails and often forms rings – polar, inclined or equatorial – that will appear as dust lanes seen edge-on. In the CO (2–1) gas distribution of NGC 1614 (Fig. 2) we found that the feature labelled *umbilical cords* appears to be associated with a dust lane northwest of the nucleus of NGC 1614, which has previously been identified with the CO (1–0) emission by Olsson et al. (2010, see also Fig. 1 in this paper). This link to the dust lane might be the connection point that fuels the starburst ring and is comparable with the twin-peak morphology in the rings of barred spiral galaxies (e.g. NGC 1097, NGC 1365, see Sect. 4.3). However, for NGC 1614 we only found one connection point, and a possible a stellar bar and its properties is still under debate (see for example the discussions in Chapelon et al. 1999; Olsson et al. 2010). This connection could be due to orbit crowding of inflowing gas streams (*umbilical cords*, traced by the CO (1–0) and the dust lane to the northwest in Fig. 1) at the branch-off of the ring, where gas encounters shocks and then migrates to new orbits where it accumulates in the shape of the starburst ring. The gas at the western and southern edges of the ring is consistent with an additional dust lane component that crosses the ring from the west to the southeast (see Fig. 1). This additional component is possibly the site of a second connection between the starburst ring and the dust lanes in this system, but this remains to be confirmed.

As observed in high-resolution CO (1–0) (Olsson et al. 2010), the starburst ring has the same velocity structure as the underlying galaxy, which we do not see because the lower surface density gas is filtered out in our high-resolution observations. Within the ring the rotation is higher than in the rest of the galaxy. The gas slows down relative to the galaxy's rotation curve toward the edges of the CO (2–1) distribution at the connection point, where the dust lane connects to the ring in the northern part. The gas distribution in the ring may be lopsided because the whole ring is fueled/fed from one side only, which might also be the reason for the asymmetry of the ring itself.

We found that the CO (2–1) emission resolved in our interferometric observations is located at the unresolved center of the larger scale molecular gas reservoir (CO (1–0)). However, with the present data sets we were unable to verify possible streaming motions between the larger scale and smaller scale molecular gas reservoirs. Therefore we are unable to determine the inflow rate of the gas. To correct this, higher resolution CO (1–0) observations are needed.

With the large reservoir of available gas in the ring and the star formation rate (SFR) of ~5.2 $M_\odot$ yr^{-1} determined from the ^{12}CO (2–1) emission, taking the gas mass in the ring and its surface density into account, the star formation in the center

of NGC 1614 could go on for another $\sim 1.6 \times 10^8$ yr unless processes/events occur that stop the gas transport via the feeding lines.

4.1.2. Formation of GMAs in the ring

In Sect. 4.1.1 we established that there is a connection between the dust lanes in NGC 1614 and the molecular ring seen in ^{12}CO 2−1 emission. Prominent features of the ring and the surrounding gaseous material are ten GMAs. In the prominent minor axis dust lane north of the ring, however, we detect no GMAs – although this is the main location of the bulk of the CO (2−1) flux (Wilson et al. 2008). Hence, the CO (2−1) emission here is either emerging from smaller molecular clouds with a surface brightness too low to be detected by us – or alternatively the molecular gas is in the form of diffuse, unbound molecular clouds that are filtered out by the lack of short-spacing baselines in our data. The latter scenario would be consistent with the increase in ^{12}CO/^{13}CO (2−1) ratio with radius reported in Sect. 3.2.4. This scenario may have similarities to that found for NGC 6946 Meier & Turner (2004), where molecular gas outside the central ring was found to be of lower density and more diffuse than the dense, self-gravitating gas in the ring. This is reflected as a rapid change in the interstellar medium (ISM) from dense star-forming cores in a central ring to diffuse, low-density molecular gas in and behind the molecular arms. This results in ^{12}CO/^{13}CO (2−1) intensity ratios in the central ring that are lower than in the diffuse gas on larger scales – which also seems to be the case for NGC 1614 (see Sect. 3.2.4). Therefore, the absence of GMAs outside the ring leeds us to conclude that the GMAs in NGC 1614 are formed as a result of some form of orbit-crowding within the nuclear ring from gas funneled from the dust lane reservoir.

Analogies for the GMA formation processes could be M 51 (Koda et al. 2009) or IC 342 (Hirota et al. 2011, see also Sect. 4.3.3 for a more detailed comparison with other GMA-bearing galaxies). In M 51 the GMAs are only found in the spiral arms. They are formed upon entering the spiral arms through coagulation triggered by spiral-arm streaming motions and are disrupted again by fragmentation upon leaving the spiral arms.

For NGC 1614 we propose the following scenario: Smaller sized GMCs are funneled along the *umbilical cords* toward the molecular ring. At the transition from the dust lane to the molecular ring we assume that crowding processes (e.g. orbital crowding) in the mergers take place that lead to the collisional coagulation of individual GMCs. These cloud-cloud collisions could also trigger the onset of star formation (Scoville et al. 1986; Tan 2000) – the dissipation of excess kinetic energy during the collisions is a prerequisite for star formation (Hirota et al. 2011). Observations at higher angular resolution and sensitivity are necessary to resolve the molecular gas properties of the low surface brightness GMCs in the *umbilical cords*.

4.2. Tracers of star formation

4.2.1. Annular profiles

In Fig. 6 we present the annular profiles of Paα, CO (2−1), radio *L*- (1.4 GHz), *C*- (5 GHz), and *X* (8.4 GHz)-band. The averaged annular profiles for the NGC 1614 ring are shown for all tracers (Fig. 6 upper left panel). We simply azimuthally averaged the flux density in a series of 0.1″-wide annular circular rings (i.e., we excluded inclination effects). We did not exclude any parts of the annulus that might be atypical in any band. We also set the ring center in the middle of the Paα where there is a slight central feature and used this position in all bands. This matches the weak *C*- and *X*-band central feature quite well.

We also divided the ring into four sections, north (N), east (E), west (W) and south (S) and plotted semi-annuli to study any positional shift in the relative radii of all five tracers (Fig. 6).

For the average annuli we see that the *L*-band profile is the tracer with the strongest relative nuclear peak. The ring (or ring-like structure) is visible in *L*-band (indicated by the step in the profile) but not quite as pronounced and possibly not with exactly the same central position. As expected, the radio *C*- and *X*-band data trace each other very well – and the ring radius may be shifted by 0.1″ compared to that of Paα – but the difference is very small and within errors. The average CO (2−1) profile is shifted outwards by 0.2″ from that of Paα. The nuclear region is obviously void of any CO (2−1) emission (that can be recovered in Vext by the SMA).

However, when inspecting the N, E, W, and S cuts, we find that there are large directional differences in the peak radii of the different tracers. All W cuts show a peak radius of 0.6″ for all tracers – the agreement is almost perfect and there is a well-defined local maximum for all tracers. In contrast, the strongest discrepancy is seen in the N cut between Paα and CO (2−1). Paα peaks at 0.3″ with a sharp profile while CO (2−1) peaks at 0.9″ with a large, rounded, extended (even double-peaked) structure. A similar but less pronounced effect can be seen in the S cut.

Part of the explanation for this discrepancy can be seen in Fig. 5 which clearly shows the north-south elongated distribution of CO (2−1) with respect to Paα. The correlation between the tracers is good in the west – but poorer in the north and south because of the additional contribution to the CO (2−1) emission that does not exclusively come from the ring itself, but also from the combined CO (2−1) contributions from the dust lane and its connection point to the ring.

The annuli are discussed in more detail in Sect. 4.3.1.

4.2.2. "Wildfire" vs. dynamics

There have been suggestions for different evolutionary tracks for the development of a starburst ring in NGC 1614. Alonso-Herrero et al. (2000) suggested a "wildfire"-like scenario in which the ring was formed by a nuclear starburst that progresses outward and already has consumed almost the whole gas in its center. In contrast to this, Olsson et al. (2010) proposed a scenario in which gas is piled up at an inner Lindblad resonance to form the ring.

Supporting the wildfire origin of the starburst ring is the fact that the Paα and the radio continuum emission are distributed consistently inside the starburst ring, as seen in CO (2−1). The same is true for 1.6 μm emission (*H*-band) observed by Haan et al. (2011). The emission is centrally peaked like the Paα and the radio continuum emission. But in contrast to the other tracers, the 1.6 μm emission is distributed in a broken-ring structure that has an opening to the northwest (Haan et al. 2011). Our observations of CO (2−1) show, however, that the molecular ring is open to the northeast. The radio continuum suggests, furthermore, that an older starburst lies in the ring center at the nucleus. An alternative explanation for the 1.4 GHz emission in the center could be an additional synchrotron component, possibly from a weak AGN. However, the distance between the tracers varies with the direction, which could also be indicative of spatial shifts between the tracers that are not caused by wildfires.

It was also suggested that the starburst ring in NGC 1614 could be caused by an inner Lindblad resonance

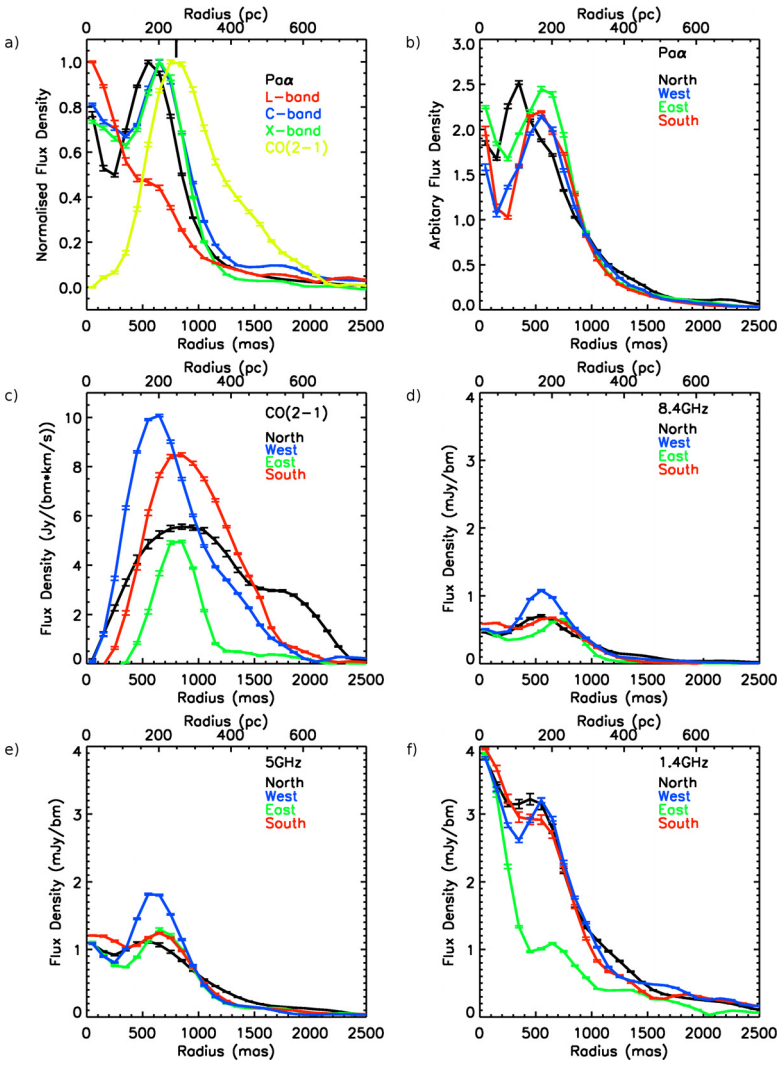

Fig. 6. Comparison of the annular profiles of the new CO (2−1) data with Paα, 8.4 GHz (X-band), 5 GHz (C-band) and 1.4 GHz (L-band) data from Olsson et al. (2010) **a)**, *top left*. These profiles, obtained by azimuthally averaging the flux density in 0.1″ wide annular circular rings, are nominally centered on the center of the Paα ring. Profiles of each tracer in different regions of the ring are presented from *top right* to *bottom left*: Paα **b)**, CO (2−1) **c)**, 8.4 GHz **d)**, 5 GHz **e)** and 1.4 GHz **f)**. Spatial resolutions of the data used for the profiles are ∼0.2″ for Paα, ∼0.3″ for the L-, C- and X-band observations and the spatial resolution for the CO data is ∼0.5″.

(Olsson et al. 2010). One might argue that this process only takes place in barred galaxies, and it is still debated whether there is a stellar bar in NGC 1614 or not (see e.g., Olsson et al. 2010, who found an oval distortion in their K-band data that is consistent with a bar). But galaxies with molecular rings have been found that have no bars (e.g. NGC 278 & NGC 7217, Knapen et al. 2004; Sarzi et al. 2007). It has been shown that other physical properties, e.g., a weak oval distortion (Buta et al. 1995), a dissolved bar (Verdes-Montenegro et al. 1995), tidal effects of a companion galaxy (Combes 1988a), or a recent minor merger (Knapen et al. 2004; Mazzuca et al. 2006) can cause the same effect as a bar: the non-axisymmetric potential caused by the bar can channel gas to the nucleus, which is slowed down near or at the inner Lindblad resonance. Elmegreen (1994) proposed a scenario in which the gravitational collapse of gas that is caught in an inner Lindblad resonance within a starburst ring, fueled by galactic bars or strong spiral arms, can lead to the formation of giant clouds with spots of intense star formation. We do see these hot spots in Figs. 1, 2, and 5. Another argument against the wildfire scenario is the asymmetry we found in the CO (2−1) emission, whereas the distribution of star formation tracers, such as Paα and radio continuum emission, is distributed very symmetrically. Conversely, Paα and the radio continuum agree very well with each other but not with the CO (2−1) distribution, which supports the idea of a wildfire because CO traces gas properties that occur earlier, i.e., farther outward, in the star formation process than those traced by Paα and the radio continuum.

An alternative theory that can possibly explain the spread in distribution of the star formation tracers was suggested by Lou et al. (2001a), Lou et al. (2001b), and Lou (2003). These authors highlight the importance of density waves in spiral galaxies as triggers for AGN and star-bursting events: a bar or companion induces spiral density waves at the inner Lindblad resonance (Lou et al. 2001a, and references therein). Lou et al. (2001b) found that fast magneto-hydrodynamic density waves (FMDWs) play an important dynamic role in developing the circumnuclear region of spiral galaxies with bars. The critical parameter seems to be the dampening of the FMDWs, which can lead to the onset of AGN activity (weak density wave dampening), to the formation of circumnuclear rings (strong dampening) and a mixture of circumnuclear and AGN activity (intermediate dampening) inside the inner Lindblad resonance. The two latter processes might play a role in NGC 1614.

In summary, there is no clear tendency toward the wildfire scenario, density waves, or the idea of a Lindblad resonance as a cause for the starburst ring in NGC 1614. From our study of the connection between the molecular gas in the ring and the galaxies dust lanes, we propose the following. Star formation in the molecular ring occurs at a Lindblad resonance and is replenished with molecular gas via the dust lanes. This is a result of orbital crowding or density wave phenomena. The morphology of the

ring as seen in Paα could be caused by a wildfire independent of this star formation. We suggest that both processes coexist at the same time, but that the molecular ring is responsible for the starburst. To be able to distinguish between the three competing models, several observations might be useful: CO (1−0) observations with a resolution higher than currently available would enable us to study the possible connection between the CO (1−0) and the CO (2−1) gas reservoirs, CO data with a higher sensitivity would provide insight into the low surface brightness gas content of NGC 1614 and would allow us to continue studying the GMA formation, and observations of shock tracers, such as SiO, would help tracing a possible outward movement of the star formation by showing the places of shocked gas within the ISM.

4.3. Comparison with other galaxies

A comparison with other galaxies, such as NGC 4194 (the Medusa merger), NGC 1097, and NGC 1365 shows that there are similarities between these different types of galaxies and NGC 1614, but also that NGC 1614 does not fit in either in the same class as the Medusa or the class of barred spiral galaxies.

4.3.1. Comparison with other dust lane minor mergers

Similar properties as seen in NGC 1614 have been found for the Medusa merger. The two systems have in common minor axis dust lanes and large amounts of molecular gas associated with thesee dust lanes (Beswick et al. 2005; Olsson et al. 2010; Aalto & Hüttemeister 2000), but not with the bulk of the star formation.

Apparently, the dust lanes are part of a feeding chain where the majority of the molecular gas has yet not engaged in star formation. However, a comparison of the CO distribution and the star formation properties shows a very different picture. in NGC 1614, which is a (S+s) minor merger, the compact CO emission is closely associated with the optical nuclear star formation (Olsson et al. 2010), while in NGC 4194, an E+S minor merger, much of the star formation is going on in super star clusters (SSCs) with a kpc-scale distribution (Weistrop et al. 2004) away from the molecular gas. No obvious correlation between these young SSCs (5−15 Myr) and the CO can be found (Aalto et al. 2010). In addition, both minor mergers have a relatively high CO/HCN line ratio (CO/HCN (NGC 1614) ∼ 43, CO/HCN (NGC 4194) ∼ 61; Costagliola et al. 2011), which indicates limited reservoirs of dense gas.

With the Vext data we recover only a fraction of the CO (2−1) emission in the center of NGC 1614. When we compare our data with the lower resolution SMA data by Wilson et al. (2008), we find that we missed almost all, ∼70%, of the CO 2−1 flux in the crossing minor axis dust lane in the north.

Possibly a large fraction of the missing flux is in the form of diffuse extended emission, associated with gas flows along the minor axis dust lane. This would be a similar situation as the one suggested for the NGC 4194 minor merger by Aalto et al. (2010).

It is still unknown whether the differences in the gas distribution and starbursts are due to different merger histories, variations in the process of merging spiral galaxies with spiral galaxies or elliptical with spiral (E+S) galaxies, or diverging properties within the evolution of mergers. A careful study of several of these objects might shed some light on their evolutionary paths.

4.3.2. Comparing NGC 1614 with galaxies with nuclear molecular rings

NGC 1614 has some features in common with local barred spiral galaxies, such as NGC 1097 and NGC 1365, but unlike NGC 1614, these galaxies are not classified as mergers. These barred spirals are so-called twin-peak galaxies because they contain nuclear molecular rings that show a double-peak structure in their molecular gas distribution perpendicular to the stellar bar, where the starburst ring and the dust lanes connect (Sakamoto et al. 2007; Hsieh et al. 2011). NGC 1614 harbors an asymmetric ring and displays at least one connection point with its dust lanes. This is comparable to the twin connection points seen in local barred spirals (Kenney et al. 1992). However, some barred spirals, such as NGC 1365, do show comparable asymmetric central starburst rings (Sakamoto et al. 2007).

The molecular gas in all three objects is associated with dust lanes close to or connected to the nuclear starburst rings. Within the rings all sources show hot spots in the CO emission that possibly contain SSCs in their early stages (Sakamoto et al. 2007). An obvious difference in the CO gas distribution in the starburst ring though is the absence of CO emission in NGC 1614 at the center of the ring, as opposed to the nuclear ring in NGC 1097. This might be an indication that the central structure in NGC 1614 is older than that in NGC 1097 and therefore the gas there is already consumed or swept away by developing stars. Another possibility is that the ring and AGN activity in NGC 1097 were caused by intermediately dampened spiral density waves (Lou 2003), whereas the dampening in NGC 1614 was strong enough only to form the starburst ring (see also Sect. 4.2.2).

With sizes (radii) of ∼700 pc and 1 kpc, the nuclear rings in NGC 1097 and NGC 1365 also have a much larger extension then that of NGC 1614 (231 pc), possibly indicating that NGC 1614 harbors a scaled-down version of a nuclear starburst ring in development caused by the merger event.

Another prominent galaxy with a molecular ring is M 82. In contrast to NGC 1614, M 82 is not a merger, but constitutes an integral part of an interacting galaxy pair together with M 81. M 82 is an edge-on starburst galaxy with a nuclear molecular ring or torus (radius ∼200 pc; Nakai et al. 1987; Shen & Lo 1995) that corresponds to current sites of star formation (Nakai et al. 1987), like in NGC 1614. In M 82 in contrast to NGC 1614, however, the star formation is also associated with SSCs (Telesco & Gezari 1992), like in NGC 4194. The molecular ring in M 82 contains less than 30% of the total molecular CO mass in M 82. The ring in NGC 1614 shows a mass fraction of 30% when taking the total CO (2−1) mass from Wilson et al. (2008). In addition, the ^{12}CO / ^{13}CO (2−1) ratios for M 82 (∼14.2, Mao et al. 2000) and NGC 1614 (>15, see Sect. 3.2.4) are quite similar. A more recent study by Weiß et al. (1999) discovered an additional CO feature in M 82 that is suggested to be a superbubble driven by a starburst in its center (Matsushita et al. 2000), similar to the wildfire mode proposed by Alonso-Herrero et al. (2001) for NGC 1614.

Yet another example is the Seyfert 1 galaxy NGC 7469, which is the companion of IC 5283 in an interacting pair of similar sized galaxies. For NGC 7469 several tracers (e.g. 5 GHz radio continuum, J, H, K imaging, PAHs, CO (2−1)) were found to be located in a circumnuclear ring/spiral arm system (Wilson et al. 1991; Mazzarella et al. 1994; Miles et al. 1994; Genzel et al. 1995; Davies et al. 2004). A comparison with the starburst and molecular rings in NGC 1614 shows some prominent similarities. The near-infrared (NIR) emission detected in the K-band

Table 4. Overview of the parameters of galaxies with molecular rings compared to NGC 1614.

Galaxy	D [Mpc]	*Hubble* Type	Merger/ interaction?	Ring radius [pc]	CO central peak?	Ring symmetry[a]	Connection to dust lane?[b]	GMAs[c] [#]	Reference
NGC 1614	64.2	SB(s)b pec	+	231	–	asym	1	10	1
NGC 1097	14.5	SB(s)b	–	700	+	sym	2	19	2, 3
NGC 1365	17.9	SB(s)b	–	1000	–	asym	2	5	4
NGC 7469	66	SBa	+[d]	800	+	asym	–	–	5
M 82	3.9	I0	+[e]	200	+	sym	–	–	6
				105×70	–	asym	–	–	7, 8

Notes. [(a)] sym = symmetric, asym = asymmetric. [(b)] A number given denotes the number of connection points of the molecular ring to dust lanes, "–" indicates that there is no information available on a possible ring-dust lane connection. [(c)] A number given denotes the number of GMAs found in the molecular rings and dust lanes, "–" indicates that there is no information available on GMAs in these objects. [(d)] Part of an interacting galaxy pair with IC 5283. [(e)] Part of an interacting galaxy pair with M 81.

References. 1) This work; 2) Hsieh et al. (2008); 3) Hsieh et al. (2011); 4) Sakamoto et al. (2007); 5) Davies et al. (2004); 6) Nakai et al. (1987); 7) Weiß et al. (1999); 8) Matsushita et al. (2000).

continuum, associated with the radio continuum and other tracers, is found inside the CO emission distribution (Davies et al. 2004). For NGC 7469 however, the CO (2−1) distribution shows a central peak/nuclear ring and a bar or pair of spiral arms that seems to connect to the central emission/circumnuclear ring itself (Davies et al. 2004). In NGC 1614 this is not the case.

4.3.3. GMAs in galaxies with nuclear molecular rings

One other property NGC 1614 shares with galaxies like NGC 1097 and NGC 1365 are hot spots (gas clumps and CO brightness temperature peaks, Sakamoto et al. 2007; Hsieh et al. 2011), so-called GMAs (Vogel et al. 1988). For NGC 1365, Sakamoto et al. (2007) found five CO hot spots with line widths (FWHM) between 60 and 90 km s^{-1} that seem to be associated with SSCs of $\sim 10^6$ $M_\odot$ (Galliano et al. 2005).

Hsieh et al. (2011) found many GMAs in the molecular ring (14 GMAs) and the dust lane (5 GMAs) of NGC 1097. They subdivided the GMAs in the molecular ring into two categories: GMAs with broad ($\sigma > 30$ km s^{-1}) and narrow ($\sigma < 30$ km s^{-1}) line dispersions. The line widths for the narrow GMAs (~ 55.1 km s^{-1}) are almost only half the line widths of broad-line GMAs (~ 102.0 km s^{-1}) but the average molecular gas mass is almost the same ($M_{\rm gas,ave}$(N1-N11) $\sim 8.1 \times 10^7$ $M_\odot$, $M_{\rm gas,ave}$(B1−B3) $\sim 9.3 \times 10^7$ $M_\odot$). The GMAs in the dust lane only have slightly more narrow line widths (~ 93.8 km s^{-1}) and slightly higher molecular gas masses ($M_{\rm gas,ave}$(D1−D5) $\sim 1.0 \times 10^8$ $M_\odot$) than the GMAs in the ring. For NGC 1614 the average line widths and masses are ~ 129.5 km s^{-1} and $M_{\rm gas,ave}$(ring) $\sim 7.0 \times 10^7$ $M_\odot$ for GMAs in the ring, and ~ 110.7 km s^{-1} and $M_{\rm gas,ave}$(outside the ring) $\sim 5.0 \times 10^7$ $M_\odot$ for GMAs outside the molecular ring (Table 3) − the average line widths are broader and the masses are slightly higher for GMAs in the ring than for those outside the ring in NGC 1614. At least two of the GMAs outside the ring in NGC 1614 are associated with dust lanes (GMA 2, GMA 5, Fig. 1). Three of the GMAs in the ring (GMA 6, GMA 7, and GMA 8) are also associated with a dust lane, and GMA 3 is located in the feeding lines that connect the molecular ring with the dust lane (Fig. 1).

Hsieh et al. (2011) also determined the sizes of their GMAs by measuring the number of pixels above a certain intensity threshold and then assuming the GMAs to be spherical to obtain diameters of the individual GMAs. The sizes of GMAs located in the ring of NGC 1097 and outside the structure differ significantly. The average size of a GMA situated in the molecular ring is ∼220 pc. GMAs that are situated outside the ring but in the dust lane in NGC 1097, however, have an average size of 269 pc, which is ∼20% larger than for GMAs in the ring. For NGC 1614, however, this seems to be less pronounced. The average size of GMAs in the ring is $\sim 259 \pm 24$ pc (assuming spherical morphology) and for GMAs outside the ring and associated with dust lanes it is $\sim 273 \pm 20$ pc. The GMAs in the ring in NGC 1614 seem to be larger than those found in NGC 1097 (Hsieh et al. 2011). Although the average spherical sizes for GMAs in and outside the ring are comparable and agree within the error limits, the sizes for the GMAs outside the ring that are associated with dust lanes are most likely overestimated. The sizes of these GMAs are measured at low surface brightnesses and therefore likely to be afflicted with larger errors. This does not change the fact that Hsieh et al. (2011) discovered that for NGC 1097, GMAs in the ring are significantly smaller than those outside the ring, whereas for NGC 1614 it is most likely the other way around, or possibly the sizes in and outside the ring are about the same. One deciding factor here might be the formation history of the starburst rings in these two galaxies − e.g., NGC 1614 is a merger, NGC 1097 is not.

We summarize the comparisons between the galaxies in this section in Table 4. This shows that NGC 1614 shares properties with several of the comparison galaxies − e.g., an assymetric molecular ring, dust lanes, GMAs, and a radial displacement between starburst and molecular rings. However, we always found significant differences as well. Therefore, NGC 1614 cannot be classified as a twin-peak galaxy, a typical barred spiral, or a typical merger of any flavor; it remains a very interesting yet puzzling object.

5. Summary

We have observed the 1.3 mm continuum and the ^{12}CO and ^{13}CO (2−1) transitions with high resolution toward the center of NGC 1614.

1. We detected an asymmetric distribution of the ^{12}CO (2−1) emission in a ring of 231 pc radius with a molecular gas mass of 8.3×10^8 $M_\odot$. The center of the ring is free of CO emission.
2. We did not detect ^{13}CO (2−1) with our observational setup. The lower limit of the ^{12}CO/^{13}CO (2−1) line ratio is 15.
3. We identified individual GMAs in the CO data cube, some associated with the ring, some associated with the dust lanes.

The GMAs in the ring have a higher dispersion and more mass than those outside the ring.

4. Molecular gas in the dust lane shows little evidence of star formation. While GMAs appear in the *umbilical-cord* connection between the dust lane and starburst ring, there is no evidence of substantial levels of star formation (e.g., Fig. 5). This behavior is suggestive of a transitory process in which GMAs form as they move toward the nuclear ring, but intense star formation only takes place once the molecular material merges into the ring.
5. There is no general consensus yet for one scenario to explain the formation of the circumnuclear ring. Considering our results, however, we suggest that the starburst ring is caused by a Lindblad resonance and fueled by gas moving via the dust lanes onto the ring.

In conclusion, we found that NGC 1614 is a good target for studying the impact of a minor merger on the state of the molecular gas and the formation of circumnuclear starburst rings. We proposed a way to explain how nuclear gas structures in minor mergers are fed. NGC 1614 may be an example of a merger where gas in tidally induced dust structures has been found to physically connect to a starbursting structure in the very nucleus of the galaxy. We also suggested that the GMAs in NGC 1614 are formed in situ in the ring through a combination of cloud-cloud collisions and crowding processes that facilitate the onset of star formation. Owing to the limited spatial resolution and surface brightness sensitivity, many questions remain to be answered, such as in which way the larger scale CO (1−0) is connected to the starburst, and if there is a connection to the proposed nuclear outflow (Olsson et al. 2010), or how the kinematics of cold molecular gas affect the evolution of star formation and nuclear activity in minor mergers in general. A more detailed study of the molecular gas content of NGC 1614 on different spatial scales is needed to address these questions. New studies with instruments such as ALMA will enable us to answer them.

Acknowledgements. We are grateful to Glen Petitpas for his help with the SMA observations and to the referee for her/his constructive comments. The Dark Cosmology Centre is funded by the Danish National Research Foundation. S.A. thanks the Swedish Research Council and the Swedish National Space Board for support. J.S.G. acknowledges partial support for this research from NSF grant AST0708967 from the University of Wisconsin-Madison. The Submillimeter Array is a joint project between the Smithsonian Astrophysical Observatory and the Academia Sinica Institute of Astronomy and Astrophysics and is funded by the Smithsonian Institution and the Academia Sinica. MERLIN is a national facility operated by The University of Manchester on behalf of the Science and Technology Facilities Council (STFC). The VLA is operated by the National Radio Astronomy Observatory, a facility of the National Science foundation operated under cooperative agreement by Associated Universities, Inc. This research has made use of the NASA/IPAC Extragalactic Database (NED) which is operated by the Jet Propulsion Laboratory, California Institute of Technology, under contract with the National Aeronautics and Space Administration. This research used the facilities of the Canadian Astronomy Data Centre operated by the National Research Council of Canada with the support of the Canadian Space Agency.

References

Aalto, S., & Hüttemeister, S. 2000, A&A, 362, 42
Aalto, S., Beswick, R., & Jütte, E. 2010, A&A, 522, A59
Alonso-Herrero, A., Rieke, M. J., Rieke, G. H., & Shields, J. C. 2000, ApJ, 530, 688
Alonso-Herrero, A., Engelbracht, C. W., Rieke, M. J., Rieke, G. H., & Quillen, A. C. 2001, ApJ, 546, 952
Beswick, R. J., Aalto, S., Pedlar, A., & Hüttemeister, S. 2005, A&A, 444, 791
Bournaud, F., Jog, C. J., & Combes, F. 2005, A&A, 437, 69
Buta, R., van Driel, W., Braine, J., et al. 1995, ApJ, 450, 593
Chapelon, S., Contini, T., & Davoust, E. 1999, A&A, 345, 81
Combes, F. 1988a, in Lecture Notes in Physics Molecular Clouds, Milky-Way and External Galaxies, eds. R. L. Dickman, R. L. Snell, & J. S. Young (Berlin: Springer Verlag), 315, 441
Combes, F. 1988b, in Galactic and Extragalactic Star Formation, eds. R. E. Pudritz, & M. Fich, NATO ASIC Proc., 232, 475
Costagliola, F., Aalto, S., Rodriguez, M. I., et al. 2011, A&A, 528, A30
Dasyra, K. M., Tacconi, L. J., Davies, R. I., et al. 2006, ApJ, 651, 835
Davies, R. I., Tacconi, L. J., & Genzel, R. 2004, ApJ, 602, 148
de Vaucouleurs, G., de Vaucouleurs, A., Corwin, Jr., H. G., et al. 1991, Third Reference Catalogue of Bright Galaxies, vols I–III (New york: Springer)
Elmegreen, B. G. 1994, ApJ, 425, L73
Galliano, E., Alloin, D., Pantin, E., Lagage, P. O., & Marco, O. 2005, A&A, 438, 803
Genzel, R., Weitzel, L., Tacconi-Garman, L. E., et al. 1995, ApJ, 444, 129
Haan, S., Surace, J. A., Armus, L., et al. 2011, AJ, 141, 100
Hirota, A., Kuno, N., Sato, N., et al. 2011, ApJ, 737, 40
Ho, L. C. 1999, Adv. Space Res., 23, 813
Hsieh, P.-Y., Matsushita, S., Lim, J., Kohno, K., & Sawada-Satoh, S. 2008, ApJ, 683, 70
Hsieh, P.-Y., Matsushita, S., Liu, G., et al. 2011, ApJ, 736, 129
Hunsberger, S. D., Charlton, J. C., & Zaritsky, D. 1996, ApJ, 462, 50
Jesseit, R., Naab, T., Peletier, R. F., & Burkert, A. 2007, MNRAS, 376, 997
Kenney, J. D. P., Wilson, C. D., Scoville, N. Z., Devereux, N. A., & Young, J. S. 1992, ApJ, 395, L79
Knapen, J. H., Whyte, L. F., de Blok, W. J. G., & van der Hulst, J. M. 2004, A&A, 423, 481
Koda, J., Scoville, N., Sawada, T., et al. 2009, ApJ, 700, L132
Kormendy, J., Fisher, D. B., Cornell, M. E., & Bender, R. 2009, ApJS, 182, 216
Lou, Y. Q. 2003, Acta Astron. Sin., 44, 172
Lou, Y.-Q., Yuan, C., & Fan, Z. 2001a, ApJ, 552, 189
Lou, Y.-Q., Yuan, C., Fan, Z., & Leon, S. 2001b, ApJ, 553, L35
Mao, R. Q., Henkel, C., Schulz, A., et al. 2000, A&A, 358, 433
Matsushita, S., Kawabe, R., Matsumoto, H., et al. 2000, ApJ, 545, L107
Mazzarella, J. M., Voit, G. M., Soifer, B. T., et al. 1994, AJ, 107, 1274
Mazzuca, L. M., Sarzi, M., Knapen, J. H., Veilleux, S., & Swaters, R. 2006, ApJ, 649, L79
Meier, D. S., & Turner, J. L. 2004, AJ, 127, 2069
Miles, J. W., Houck, J. R., & Hayward, T. L. 1994, ApJ, 425, L37
Monreal-Ibero, A., Arribas, S., & Colina, L. 2006, ApJ, 637, 138
Nakai, N., Hayashi, M., Handa, T., et al. 1987, PASJ, 39, 685
Narayanan, D., Krumholz, M., Ostriker, E. C., & Hernquist, L. 2011, MNRAS, 418, 664
Neff, S. G., Hutchings, J. B., Standord, S. A., & Unger, S. W. 1990, AJ, 99, 1088
Olsson, E., Aalto, S., Thomasson, M., & Beswick, R. 2010, A&A, 513, A11
Puxley, P. J., & Brand, P. W. J. L. 1999, ApJ, 514, 675
Sakamoto, K., Ho, P. T. P., Mao, R.-Q., Matsushita, S., & Peck, A. B. 2007, ApJ, 654, 782
Sanders, D. B., Mazzarella, J. M., Kim, D.-C., Surace, J. A., & Soifer, B. T. 2003, AJ, 126, 1607
Sarzi, M., Allard, E. L., Knapen, J. H., & Mazzuca, L. M. 2007, MNRAS, 380, 949
Scoville, N. Z., Soifer, B. T., Neugebauer, G., et al. 1985, ApJ, 289, 129
Scoville, N. Z., Sanders, D. B., & Clemens, D. P. 1986, ApJ, 310, L77
Shen, J., & Lo, K. Y. 1995, ApJ, 445, L99
Shlosman, I., Frank, J., & Begelman, M. C. 1989, Nature, 338, 45
Simkin, S. M., Su, H. J., & Schwarz, M. P. 1980, ApJ, 237, 404
Somerville, R. S., Hopkins, P. F., Cox, T. J., Robertson, B. E., & Hernquist, L. 2008, MNRAS, 391, 481
Stutzki, J., & Guesten, R. 1990, ApJ, 356, 513
Tacconi, L. J., Genzel, R., Lutz, D., et al. 2002, ApJ, 580, 73
Tan, J. C. 2000, ApJ, 536, 173
Telesco, C. M., & Gezari, D. Y. 1992, ApJ, 395, 461
Terashima, Y., Ho, L. C., Ptak, A. F., et al. 2000, ApJ, 533, 729
Toomre, A., & Toomre, J. 1972, ApJ, 178, 623
Toth, G., & Ostriker, J. P. 1992, ApJ, 389, 5
Väisänen, P., Rajpaul, V., Zijlstra, A. A., Reunanen, J., & Kotilainen, J. 2012, MNRAS, 420, 2209
Veilleux, S., Sanders, D. B., & Kim, D.-C. 1999, ApJ, 522, 139
Verdes-Montenegro, L., Bosma, A., & Athanassoula, E. 1995, A&A, 300, 65
Vogel, S. N., Kulkarni, S. R., & Scoville, N. Z. 1988, Nature, 334, 402
Weiß, A., Walter, F., Neininger, N., & Klein, U. 1999, A&A, 345, L23
Weistrop, D., Eggers, D., Hancock, M., et al. 2004, AJ, 127, 1360
Wilson, A. S., Helfer, T. T., Haniff, C. A., & Ward, M. J. 1991, ApJ, 381, 79
Wilson, C. D., Petitpas, G. R., Iono, D., et al. 2008, ApJS, 178, 189
Zaritsky, D. 1995, ApJ, 448, L17